Pulsed quadrature-phase squeezing of solitary waves in $\chi^{(2)}$ parametric waveguides

M. J. Werner
NTT Basic Research Laboratories, 3-1 Morinosato-Wakamiya, Atsugi, Kanagawa 243-01, Japan

P. D. Drummond
Department of Physics, University of Queensland, St. Lucia, 4072 Brisbane, Australia
(Received 24 January 1997)

It is shown that coherent quantum simultons (simultaneous solitary waves at two different frequencies) can undergo quadrature-phase squeezing as they propagate through a dispersive $\chi^{(2)}$ waveguide. This requires a treatment of the coupled quantized fields including a quantized depleted pump field. A technique involving nonlinear stochastic parabolic partial differential equations using a nondiagonal coherent state representation in combination with an exact Wigner representation on a reduced phase space is outlined. We explicitly demonstrate that group-velocity matched $\chi^{(2)}$ waveguides which exhibit collinear propagation can produce quadrature-phase squeezed simultons. Quasi-phase-matched KTP waveguides, even with their large group-velocity mismatch between fundamental and second harmonic at 425 nm, can produce 3 dB squeezed bright pulses at 850 nm in the large phase-mismatch regime. This can be improved to more than 6 dB by using group-velocity matched waveguides. [S1050-2947(97)06707-3]

PACS number(s): 42.50.Dv, 42.65.Tg, 42.50.Lc

I. INTRODUCTION

Recently there has been a renewed interest in $\chi^{(2)}$ quadratic media due to the realization that optical solitary waves can propagate in the presence of dispersion (or diffraction). This has been known for a long time but it is only recently that the earlier work was recognized and extended. The theoretical efforts in the last few years have led to a much greater understanding of the extent of possible solutions and their stability. The related research on cascading in $\chi^{(2)}$ materials has demonstrated possible applications of $\chi^{(2)}$ waveguides through the ability to induce large nonlinear phase shifts [1]. These solitary waves, called simultons, in quadratic media are quite different from the well-known solitons of the nonlinear Schrödinger equation. Simulton stability properties have been investigated [2] along with their behavior during collisions [3] and their quantum counterparts—coherent quantum simultons [4]. This paper demonstrates that coherent quantum simultons can exhibit quadrature-phase squeezing [5] due to propagation through the dispersive $\chi^{(2)}$ waveguide.

The optical field propagation of solitary waves [6–9] called simultons [3,10,11] has been theoretically predicted to occur under a variety of conditions and observed experimentally as spatial solitons or self-guided waves in three dimensions [12]. Temporal $(1+1)$ dimensional forms have not been experimentally verified yet, but promising candidates to achieve the material parameter requirements are currently available [13]. The favored materials in recent experiments on second-harmonic generation of short pulses were BBO [14] and quasi-phase-matched $LiNBO_3$ [15]. The latter material has been used previously for squeezing experiments [16] and can be phase-velocity and group-velocity matched near 1.6 μm [13]. In the former case the commonly used crystal BBO is well matched near 1.5 μm with respect to group-velocity, however, it is not 90° phase matched. A recent paper has shown that solitary waves exist under a variety of conditions even when birefringence is present [17]. The observation of temporal solitary waves, though more difficult than spatial forms, is therefore a possibility in the future.

In the past ten years, the use of silica fiber as an optical single transverse mode waveguide for demonstrating quantum effects of nonlinear optical processes has been very successful [18]. The quantum noise effects of propagating coherent quantum solitons through silica fiber have been demonstrated in a number of experiments. In addition to being the first experiments on quantum solitons, the physics investigated has been of practical use in understanding the limits imposed on optical communication channels by quantum noise. A major disadvantage of this medium for some applications is the long interaction lengths typically required which makes monolithic integration difficult. There are also the acoustic and optical phonons of the silica fiber which lead to Brillouin and Raman scattering. To circumvent the weak interaction of the silica fiber with light, $\chi^{(3)}$ analogs using $\chi^{(2)}$ materials have been investigated. More generally, cascaded $\chi^{(2)}$ processes have led to qualitatively different behavior than just intensity-dependent phase shifts due to the three-wave mixing processes involved. Consequently, the quantum noise effects of propagating coherent pulses through $\chi^{(2)}$ media can also be qualitatively different from those observed in $\chi^{(3)}$ media. However, in the limiting case of a large phase mismatch similar behavior is expected.

Traveling-wave parametric amplifiers are phase-sensitive amplifiers where in general three-wave mixing processes via a $\chi^{(2)}$ nonlinearity include parametric down-conversion, second-harmonic generation, and effective $\chi^{(3)}$ processes via cascaded $\chi^{(2)}$ interactions. Quantum continuous-wave $\chi^{(2)}$ processes have been revisited again recently by Li and Kumar [19,20]. There the conclusion was that quadrature-phase

squeezing was associated with amplification of the fundamental and amplitude squeezing was associated with deamplification of the fundamental. Also, it was shown that in second-harmonic generation the quadrature-phase squeezing of the harmonic field is limited to 50% when exact phase matching is used [19]. This paper describes a robust algorithm for calculating quantum statistics of parametric processes in $\chi^{(2)}$ waveguides, including pulsed inputs and dispersion; in particular, we shall treat the subshot noise level spectral fluctuations observed in recent experiments on ultrashort pulsed squeezing in parametric waveguides [21].

We also investigate the quantum noise generated by the parametric soliton, or ''simulton,'' solutions of the $\chi^{(2)}$ interaction including linear dispersion. Previous work published on temporal simultons treated the classical field propagation problem of stable pulse formation, whereas we are interested in the quantum statistics of initial coherent forms of these solutions. Little is known about the quantum noise properties of simultons. The techniques described in this paper and elsewhere [22] can be used to predict the quantum statistics of coherent quantum simultons and generalizations of the Hamiltonian to include other nonlinear processes. At a more fundamental level, theoretical predictions of nonclassical photon correlations provide a test of the quantum theoretic and computational methods used for describing quantum field propagation in dispersive nonlinear dielectrics.

The stochastic partial differential equations which describe the evolution of the photon flux amplitudes are derived in Sec. II. These are used to formulate a hybrid positive-P–Wigner stochastic partial differential equations in Sec. III, which can be used for efficient calculations of the correlation functions of interest. Here the correlation function required is the quadrature-phase squeezing spectrum which is derived in Sec. IV. The methods used to integrate the stochastic partial differential equations and generate the correlation functions have been described in detail elsewhere [22]. The results for quantum squeezing in down-conversion and for coherent simulton propagation are presented in Sec. V. Finally we provide concluding remarks in Sec. VI.

II. QUANTUM THEORY FOR $\chi^{(2)}$ WAVEGUIDES

The traveling-wave parametric amplifier is modeled here as a nonlinear, dispersive dielectric waveguide which allows propagation in the z direction in single transverse modes for both the fundamental (signal) and second harmonic (pump). We assume that the waveguide is oriented such that type-I phase matching for the $\chi^{(2)}$ process is dominant. This restriction is imposed since only a single polarization mode for each field is included for simplicity. It is trivial to generalize to type-II phase matching for collinear propagation. Birefringence is not included here, so the phase matching should be such that there is no walk off between the ordinary and extraordinary fields. The problem of (3+1) dimensional propagation in the paraxial approximation using Hermite-Gaussian modes has been treated [4] and will appear elsewhere. The Hamiltonian used here is the same as appears in the earlier work of Raymer *et. al.* [23],

$$\hat{H}=\sum_m \hbar\omega_m^{(1)}\hat{a}_m^{(1)\dagger}\hat{a}_m^{(1)}+\sum_m \hbar\omega_m^{(2)}\hat{a}_m^{(2)\dagger}\hat{a}_m^{(2)} - \frac{1}{3}\epsilon_0\chi^{(2)}\int d^3x:\left[\frac{\hat{D}^{(1)}(\mathbf{x})}{\epsilon_1}+\frac{\hat{D}^{(2)}(\mathbf{x})}{\epsilon_2}\right]^3:, \quad (2.1)$$

where the notation : : represents normal ordering. Here the electric displacements $D^{(i)}(\mathbf{x})$ in the nonlinear term are expanded in terms of the boson field operators as

$$\hat{D}^{(i)}(\mathbf{x})=i\sum_m\left(\frac{\epsilon_i\hbar\omega_i' k_0^{(i)}}{2L}\right)^{1/2}\hat{a}_m^{(i)}u^{(i)}(\mathbf{x})\exp(ik_m^{(i)}z)+\text{H.c.}, \quad (2.2)$$

where the frequency dependence of the parameters has been kept only for the phase-shift term $\exp(ik_m^{(i)}z)$. The electric permittivity at the frequencies ω_1 and $\omega_2=2\omega_1$ are given by ϵ_1 and ϵ_2, with corresponding carrier frequency wave numbers $k_0^{(i)}=k(\omega_i)$, and group velocities $\omega_i'=\partial\omega(k_0^{(i)}/\partial k$.

The annihilation operators $\hat{a}_m^{(i)}$ correspond to a mode with propagation constant

$$k_m^{(i)}=\left(\frac{\epsilon_i}{\epsilon_0}\right)^{1/2}\frac{\omega_i}{c}+m\Delta k, \quad m=-M,\ldots,M \quad (2.3)$$

with mode spacing $\Delta k=2\pi/L$. The mode volume is then defined by the normalized transverse mode function $u^{(i)}(\mathbf{x})$ and the length L of the medium. Here $\mathbf{x}$ represents the transverse coordinates. The mode frequencies $\omega_m^{(i)}$ are approximate, corresponding to a second-order Taylor expansion, so that

$$\omega_m^{(i)}\approx\omega_i+(m\Delta k)\omega_i'+\tfrac{1}{2}(m\Delta k)^2\omega_i'', \quad (2.4)$$

where the derivatives ω_i' and ω_i'' are with respect to k. This is easily extended to include higher-order dispersion if desired. The procedure for transforming to local field operators has been given in the work of Drummond and Carter [24]. The local field operators are defined on a lattice of length L with $2M+1$ points by

$$\hat{\alpha}_l=\frac{1}{\sqrt{2M+1}}\sum_{m=-M}^{M}\hat{a}_m^{(1)}\exp\left(\frac{i2\pi ml}{2M+1}-i\omega t\right) \quad (2.5)$$

so that the lattice cell denoted by l corresponds to longitudinal position $z_l=l\Delta z=lL/(2M+1)$. Local operators $\hat{\beta}_l$ are defined analogously from the $\hat{a}_m^{(2)}$ operators. The effective Hamiltonian for the time evolution of α_l,β_l can be written in an interaction picture, which removes the carrier frequency oscillations, as

$$\hat{H}/\hbar=\sum_l\sum_{l'}\Delta\omega_{ll'}^{\alpha}\hat{\alpha}_l^{\dagger}\hat{\alpha}_{l'}+\sum_l\sum_{l'}\Delta\omega_{ll'}^{\beta}\hat{\beta}_l^{\dagger}\hat{\beta}_{l'} +\frac{i}{2}\sum_l\chi_l^{*}\hat{\alpha}_l^{\dagger 2}\hat{\beta}_l+\text{H.c.}, \quad (2.6)$$

where the definition of $\Delta\omega_{ll'}$ follows directly [24] from substituting Eq. (2.5) into Eq. (2.1) and we define

$$\chi_l=\chi\omega_1'\left(\frac{\omega_2'}{\Delta z}\right)^{1/2}e^{i(2k_0^{(1)}-k_0^{(2)})z_l}. \tag{2.7}$$

Here, for later use, we introduce a traveling-wave nonlinear coefficient defined as

$$\chi=\frac{\epsilon_0\chi^{(2)}k_0^{(1)}}{\epsilon_1}\left(\frac{\hbar k_0^{(2)}}{2\epsilon_2}\right)^{1/2}\int d^2\mathbf{x}(u^{(1)}(\mathbf{x}))^2u^{(2)*}(\mathbf{x}). \tag{2.8}$$

A. Phase-space representations

Phase-space representations of operator equations allow the development of a theory that is equivalent to the standard Heisenberg operator equations of motion, but is more readily soluble.

There are two common approaches to obtaining the phase-space equations of motion for the electromagnetic field with nonclassical statistics. The first of these is based on an expansion of the density operator in terms of nondiagonal coherent state projection operators. This normally ordered phase-space method, known as the positive-*P* representation, has proved to be useful in cases of non-classical statistics. It leads to a set of four stochastic *c*-number equations equivalent to the *quantum* equations, which also reproduce the *classical* equations in the limit of small quantum effects, or large photon number.

This technique is related to the Glauber-Sudarshan [25] *P* representation, but this diagonal expansion method has a singular behavior for this Hamiltonian. Accordingly, a nondiagonal coherent state expansion of the density matrix is preferable. The result is a generalized *P* representation Fokker-Planck equation, which is an extension of the diagonal Glauber-Sudarshan *P* representation.

A number of different types of generalized *P* representation are known [26]. Here the positive-*P* representation will be used, which is able to treat all types of nonclassical radiation as a positive distribution on a nonclassical phase space, and is amenable to numerical simulation using stochastic equations. Using this method, the operator equations are transformed to complex Ito stochastic equations, which only involve *c*-number (commuting) variables. Thus, while quantum effects require that the usual classical equation be reinterpreted as an operator equation, the operator equation in turn can be transformed to equivalent *c*-number stochastic equations.

The other phase-space representation involves analyzing the problem in terms of the Wigner function, by truncating third-order derivatives in the corresponding evolution equation for the Wigner distribution. The *approximate* truncation generates another *c*-number stochastic equation for the field which closely resembles the classical equation. However, the classical resemblance is due to the truncation process—which effectively reduces the exact quantum-mechanical Wigner equation to a semiclassical form.

Generally, in these operator representation methods, an equivalent classical field ϕ is introduced with

$$\langle\phi\rangle_{\text{stochastic}}=\langle\hat{\phi}\rangle_{\text{quantum}}. \tag{2.9}$$

Correlations of just one chosen ordering can be represented directly. Thus correction terms are needed for alternate orderings. The coherent state methods correspond to normally ordered correlations (like direct photodetection), while the Wigner method corresponds to symmetrically ordered correlations (like local-oscillator homodyne detection). In both cases, correction terms can be included to treat alternate operator orderings. For example, the Wigner method leads to a stochastic field that includes vacuum fluctuation terms. These are not physically measured by normal photodetectors, so a (small) correction term that depends on the frequency cutoff is needed for comparisons with experimentally measured spectra, especially at low intensity.

When linearization about a mean intense field is difficult (as in the case of pulsed inputs which may have no exact solution under the influence of dispersion and nonlinearity) it is therefore possible to numerically simulate the stochastic equations using one of these operator representations. The results of this procedure will be given in the following sections of the paper.

The purpose here is thus to explain the nature of the coupled stochastic equations obtained using various phase-space representations for the behavior of the propagating electromagnetic field. While these techniques are particularly useful when the linearized approximations for the Heisenberg equations break down, one can also view them as giving a justification of these methods, since operator linearization is not a very well-defined procedure. The chief advantage of these methods, relative to conventional number state expansions, is that number state techniques tend to become very rapidly unwieldy with large photon numbers and lattice sizes, due to the enormous size of the Hilbert space — which is precisely the typical situation here.

The corresponding Ito stochastic differential equations (SDE's) are (consider the parameter s to be restricted to $\{0,1\}$ where $s=1$ corresponds to the positive-*P* representation and $s=0$ to the Wigner representation)

$$\frac{\partial\alpha_l}{\partial t}=-i\sum_{l'}\Delta\omega_{ll'}^{\alpha}\alpha_{l'}+\chi_l^*\alpha_l^\dagger\beta_l+s\sqrt{\chi_l^*\beta_l}\zeta_l(t),$$

$$\frac{\partial\alpha_l^\dagger}{\partial t}=+i\sum_{l'}\Delta\omega_{l'l}^{\alpha}\alpha_{l'}^\dagger+\chi_l\alpha_l\beta_l^\dagger+s\sqrt{\chi_l\beta_l^\dagger}\zeta_l^\dagger(t),$$

$$\frac{\partial\beta_l}{\partial t}=-i\sum_{l'}\Delta\omega_{ll'}^{\beta}\beta_{l'}-\frac{1}{2}\chi_l\alpha_l^2,$$

$$\frac{\partial\beta_l^\dagger}{\partial t}=+i\sum_{l'}\Delta\omega_{l'l}^{\beta}\beta_{l'}^\dagger-\frac{1}{2}\chi_l^*\alpha_l^{\dagger 2}, \tag{2.10}$$

where the noises are real Gaussian stochastic processes with correlations given by

$$\langle\zeta_l(t)\zeta_{l'}(t')\rangle=\delta_{ll'}\delta(t-t'),$$

$$\langle\zeta_l(t)\zeta_{l'}^\dagger(t')\rangle=\langle\zeta_l(t)\rangle=\langle\zeta_l^\dagger(t)\rangle=0.$$

While these equations are stochastic for the positive-P case, and deterministic for the truncated Wigner case, the reverse is true for the initial conditions of these equations—which are always stochastic in the Wigner case. The initial conditions in the case of an initial coherent state amplitude α_l^C, β_l^C are $\alpha_l^\dagger = \alpha_l^*, \beta_l^\dagger = \beta_l^*$, with

$$\langle \alpha_l(t) \rangle = \alpha_l^C,$$

$$\langle \beta_l(t) \rangle = \beta_l^C. \tag{2.11}$$

In the case of the positive -P representation since the basis set is coherent, there are not additional fluctuations needed to represent an initial coherent state. This is not the case for the Wigner representation, which must include random fluctuations to represent any coherent state–including the vacuum state:

$$\langle \Delta A_l(t) \Delta \alpha_{l'}^\dagger(t') \rangle = \frac{1-s}{2} \delta_{ll'} \delta(t-t'),$$

$$\langle \Delta \beta_l(t) \Delta \beta_{l'}^\dagger(t') \rangle = \frac{1-s}{2} \delta_{ll'} \delta(t-t'). \tag{2.12}$$

It is important to note that in the positive-P representation $\alpha_l^\dagger(\beta_l^\dagger)$ is not necessarily the complex conjugate of $\alpha_l(\beta_l)$ except in the mean. The derivation of the Fokker-Planck equation for $W(\boldsymbol{\alpha}, \boldsymbol{\beta}; s, t)$ [27] and $P(\boldsymbol{\alpha}; t)$ [26] relies upon the use of partial integration, and assumes the distribution is sufficiently rapidly vanishing at the phase-space boundaries where $|\alpha_l|, |\beta_l| \to \infty$. This assumption is not always valid [28], in which case the stochastic method is asymptotic at small coupling constant, rather than exact. The boundary terms can be checked in each case simply by monitoring the trajectories for large departures towards infinity; these were not observed for the parameters relevant to the present simulations.

The equivalence between a Fokker-Planck equation with second-order derivatives and stochastic differential equations also requires a positive semidefinite diffusion. However, an evolution equation for the positive-P distribution ($s=1$) can always be found such that it has a positive semidefinite diffusion using the nonuniqueness of the time development of $P(\boldsymbol{\alpha}; t)$ corresponding to the original master equation [26]. Although the exact Wigner distribution equations have third-order derivative terms which must be truncated, these do not occur in the case of the positive-P representation, so no additional assumptions are needed to transform the Fokker-Planck equation into stochastic equations.

Either type of equation can be transformed to evolve photon flux amplitudes by defining

$$\Phi_l = \alpha_l \left(\frac{\omega_1'}{\Delta z} \right)^{1/2}, \quad \Psi_l = \beta_l \left(\frac{\omega_2'}{\Delta z} \right)^{1/2} e^{i(2k_0^{(1)} - k_0^{(2)}) z_l} \tag{2.13}$$

where $\Phi_l^\dagger \Phi_l - (1\text{-}s)\omega_1'/(2\Delta z)$ and $\Psi_l^\dagger \Psi_l - (1\text{-}s)\omega_2'/(2\Delta z)$ equal the number of photons per second passing the z_l plane for signal and pump fields, respectively. We note that the positive-P equations can be used to obtain the flux directly (it is a normally ordered representation), while the Wigner trajectories must include operator-ordering corrections to obtain the flux.

These equations can be cast into the following dimensionless equations:

$$\frac{\partial \phi}{\partial \xi} = -\frac{i}{2} \mathrm{sgn}(k_1'') \frac{\partial^2}{\partial \tau^2} \phi + \phi^\dagger \psi + s\sqrt{\psi} \zeta(\xi, \tau),$$

$$\frac{\partial \phi^\dagger}{\partial \xi} = +\frac{i}{2} \mathrm{sgn}(k_1'') \frac{\partial^2}{\partial \tau^2} \phi^\dagger + \phi \psi^\dagger + s\sqrt{\psi^\dagger} \zeta^\dagger(\xi, \tau),$$

$$\frac{\partial \psi}{\partial \xi} = \left[\frac{z_0}{t_0} \left(\frac{1}{\omega_1'} - \frac{1}{\omega_2'} \right) \frac{\partial}{\partial \tau} + i z_0 (k_0^{(2)} - 2k_0^{(1)}) - \frac{i}{2} \frac{k_2''}{|k_1''|} \left(\frac{\omega_2'}{\omega_1'} \right)^2 \frac{\partial^2}{\partial \tau^2} \right] \psi - \frac{1}{2} \phi^2,$$

$$\frac{\partial \psi^\dagger}{\partial \xi} = \left[\frac{z_0}{t_0} \left(\frac{1}{\omega_1'} - \frac{1}{\omega_2'} \right) \frac{\partial}{\partial \tau} - i z_0 (k_0^{(2)} - 2k_0^{(1)}) + \frac{i}{2} \frac{k_2''}{|k_1''|} \left(\frac{\omega_2'}{\omega_1'} \right)^2 \frac{\partial^2}{\partial \tau^2} \right] \psi^\dagger - \frac{1}{2} \phi^{\dagger 2}, \tag{2.14}$$

where $t_v = t - z/v, k_i'' = d^2k/d\omega^2|_{k=k_i} = -\omega_i''/v^3$, and t is the time measured in the laboratory frame while t_v is the time measured in the comoving frame with speed $v = \omega_1'$. The factor $(k_0^{(2)} - 2k_0^{(1)})$ accounts for any mismatch of phase velocities, while $\Delta v_3 = (z_0/t_0)(1/\omega_2' - 1/\omega_1')$ accounts for group-velocity mismatch, and k_i'' accounts for group-velocity dispersion (GVD). $\xi = z/z_0$ is the propagation distance scaled by z_0 and $\tau = t_v/t_0$ is the scaled time in the comoving frame. Here $z_0 = |\chi \Psi_0|^{-1}$ is the classical undepleted pump gain length and $t_0 = \sqrt{z_0 k_1''}$ is the inverse phase-matching bandwidth when Ψ_0 is the initial peak value of Ψ. The noise correlation is

$$\langle \zeta(\xi, \tau) \zeta(\xi', \tau') \rangle = \frac{1}{\bar{n}} \delta(\xi - \xi') \delta(\tau - \tau'). \tag{2.15}$$

where $\bar{n} = \Psi_0^2 t_0$ is the parameter governing the system size expansion. The dimensionless fields ϕ and ψ are defined by $(\phi, \psi) = (\Phi, \Psi)/\Psi_0$. In simulating quantum pulse propagation, either type of representation can be used, and is often quite suitable. The positive-P representation is particularly suitable for calculating intensities, as it is a normally-ordered representation. When calculating highly squeezed quadrature fluctuations with local oscillators, it is sometimes the case that the intrinsic sampling error can cause problems, due to the very low level of quantum fluctuations in a squeezed quadrature. This problem is reduced in the case of the Wigner representation, which tends to have lower sampling errors for quadrature squeezed states [29]. However, the truncated Wigner representation equations have another difficulty; since the equations involve a truncation, it is not clear when they actually give correct answers. It would be very useful to have a stochastic method that would combine the intrinsic accuracy of the positive-P method, with a low sampling error.

III. HYBRID WIGNER–POSITIVE-*P* SIMULATIONS

As stated in the preceding section, correct quantum statistics including a quantized pump is given by the positive-*P* representation. However, for highly nonclassical states the doubled dimensionality of the phase space can result in poor sampling statistics. The Wigner representation on the other hand describes the dynamics exactly for a classical pump on the reduced phase space where the stochastic fields representing the Hermitian conjugate field are in fact exactly the complex conjugate field. This fact can be utilized to provide a significant improvement in the sampling statistics for the positive-*P* representation for a quantized pump. Instead of directly calculating the squeezing spectrum including the effects of pump depletion and fluctuations in the positive-*P* representation, one calculates the difference between the squeezing spectrum for a classical undepleted pump and a quantized, depleted pump. It is essential to keep the noise trajectories the same in both positive-*P* simulations in order to reduce sampling errors. The Wigner representation is used to calculate the squeezing spectrum for a classical undepleted pump which is exact, as explained above. The addition of the positive-*P* difference spectra and the Wigner spectra is then the correct quantum statistics including quantized pump.

The important feature is that the sampling error is considerably smaller than in the case of the positive-*P* representation used alone, without incurring the problem of an unknown truncation error if the truncated (''semiclassical'') Wigner equations are used by themselves. While there is still the potential problem of the positive-*P* boundary correction terms, these are typically negligible under most experimental conditions, and are easily checked by monitoring the numerical trajectories for large excursions.

The hybrid Wigner–positive-*P* method for the dynamics of the $\chi^{(2)}$ interaction can be obtained from Eq. (2.14) by writing down the appropriate stochastic equations for the positive-*P* stochastic differencing and the classical pump Wigner equations. These are given by the following coupled equations for the dynamics of the $\chi^{(2)}$ interaction:

$$\frac{\partial\phi_w}{\partial\xi}=-\frac{i}{2}\mathrm{sgn}(k_1'')\frac{\partial^2}{\partial\tau^2}\phi_w+\phi_w^*\psi_c, \tag{3.1}$$

$$\frac{\partial\psi_c}{\partial\xi}=\left[\frac{z_0}{t_0}\left(\frac{1}{\omega_1'}-\frac{1}{\omega_2'}\right)\frac{\partial}{\partial\tau}+iz_0(k_0^{(2)}-2k_0^{(1)})-\frac{i}{2}\frac{k_2^{c\prime\prime}}{|k_1''|}\left(\frac{\omega_2'}{\omega_1'}\right)^2\frac{\partial^2}{\partial\tau^2}\right]\psi_c, \tag{3.2}$$

$$\frac{\partial\phi_1}{\partial\xi}=-\frac{i}{2}\mathrm{sgn}(k_1'')\frac{\partial^2}{\partial\tau^2}\phi_1+\phi_1^\dagger\psi+\sqrt{\psi}\zeta(\xi,\tau), \tag{3.3}$$

$$\frac{\partial\phi_1^\dagger}{\partial\xi}=+\frac{i}{2}\mathrm{sgn}(k_1'')\frac{\partial^2}{\partial\tau^2}\phi_1^\dagger+\phi_1\psi^\dagger+\sqrt{\psi^\dagger}\zeta^\dagger(\xi,\tau), \tag{3.4}$$

$$\frac{\partial\psi}{\partial\xi}=\left[\frac{z_0}{t_0}\left(\frac{1}{\omega_1'}-\frac{1}{\omega_2'}\right)\frac{\partial}{\partial\tau}+iz_0(k_0^{(2)}-2k_0^{(1)}),-\frac{i}{2}\frac{k_2''}{|k_1''|}\left(\frac{\omega_2'}{\omega_1'}\right)^2\frac{\partial^2}{\partial\tau^2}\right]\psi-\frac{1}{2}\phi_1^2, \tag{3.5}$$

$$\frac{\partial\psi^\dagger}{\partial\xi}=\left[\frac{z_0}{t_0}\left(\frac{1}{\omega_1'}-\frac{1}{\omega_2'}\right)\frac{\partial}{\partial\tau}-iz_0(k_0^{(2)}-2k_0^{(1)})+\frac{i}{2}\frac{k_2''}{|k_1''|}\left(\frac{\omega_2'}{\omega_1'}\right)^2\frac{\partial^2}{\partial\tau^2}\right]\psi^\dagger-\frac{1}{2}\phi_1^{\dagger 2}, \tag{3.6}$$

$$\frac{\partial\phi_2}{\partial\xi}=-\frac{i}{2}\mathrm{sgn}(k_1'')\frac{\partial^2}{\partial\tau^2}\phi_2+\phi_2^\dagger\psi_c+\sqrt{\psi_c}\zeta(\xi,\tau), \tag{3.7}$$

$$\frac{\partial\phi_2^\dagger}{\partial\xi}=+\frac{i}{2}\mathrm{sgn}(k_1'')\frac{\partial^2}{\partial\tau^2}\phi_2^\dagger+\phi_2\psi_c^*+\sqrt{\psi_c^*}\zeta^\dagger(\xi,\tau), \tag{3.8}$$

where the classical undepleted pump ψ_c has been utilized in the evolution of ϕ_2. These stochastic fields then correspond to different operator orderings and different dimensional phase spaces. That is, ϕ_2 represents a restriction of ϕ_1 to the reduced phase space $(\phi_1,\phi_1^\dagger,\psi,\psi^*)$. The homodyne detector uses a coherent local oscillator which is considered classical in the Wigner simulation and quantized in the positive-*P* simulation. Solving these six positive-*P* Ito stochastic, one Wigner, and one classical parabolic partial differential equations turns out to be more efficient than solving just the $(\phi,\phi^\dagger,\psi,\psi^\dagger)$ coupled positive-*P* equations alone.

The coupled equations above can be extended to treat a Sagnac loop interferometer analagous to the fiber loop squeezing experiments by Rosenbluh and Shelby in silica fiber [30]. In this case the local oscillator for the homodyne detector is one of the bright output pulses of a balanced Sagnac interferometer, depending upon at which frequency the quantum correlations are to be measured. A similar procedure as above is performed for each arm of the Sagnac interferometer to calculate the dynamics of the two independent counterpropagating simulton fields.

IV. SQUEEZING SPECTRUM

The time-ordered, normally ordered current operators provide the usual *N*-photon coincident rates

$$G^{(N)}(t_1,\ldots,t_N)=\langle:\hat{I}_{(t_1)}\cdots\hat{I}_{(t_N)}:\rangle \tag{4.1}$$

such that the normalized photocurrent spectrum is given by [31]

$$\overline{G(\omega,\omega')}=\sqrt{2\pi}G^{(1)}(\omega+\omega')+2\pi G^{(2)}(\omega,\omega'), \tag{4.2}$$

where

$$G^{(2)}(\omega,\omega')=\frac{1}{2\pi}\int\int e^{i\omega t+i\omega' t'}G^{(2)}(t,t')\,dt\,dt'. \tag{4.3}$$

We can rewrite the normalized photocurrent spectrum in terms of the current operators as

$$\overline{G}(\omega,\omega')=\int e^{i(\omega+\omega')t}\langle\hat{I}(t)\rangle dt+\int\int e^{i(\omega t+\omega' t')}\times\langle:\hat{I}(t)\hat{I}(t'):\rangle dt\,dt'. \tag{4.4}$$

The second term can exhibit nonclassical correlations.

Now consider a homodyne detector with two input ports a and b so that the difference current operator is

$$\hat{I}_-=(\eta_a r^2-\eta_b t^2)\Phi_a^\dagger\Phi_a+(\eta_1 t^2-\eta_b r^2)\Phi_b^\dagger\Phi_b+rt(\eta_a+\eta_b)(\Phi_a^\dagger\Phi_b+\Phi_b^\dagger\Phi_a). \tag{4.5}$$

where η_i are the detector efficiencies. We only consider a balanced homodyne detector where one has $r=t=1/\sqrt{2}$ and $\eta_a=\eta_b=\eta$. In a time interval T, the average signal observed is

$$\overline{I_-^c}=\frac{1}{T}\int_{-T/2}^{+T/2}\langle\hat{I}_-(t)\rangle dt. \tag{4.6}$$

Experiments are usually carried out not at dc but at some convenient rf frequency to avoid the local-oscillator bandwidth, electronic, and other noise (for example, mode locking frequency). The ability to measure the dc photon difference number in pulsed systems has been demonstrated experimentally [21].

We define the generalized quadrature operator as

$$\hat{X}=\gamma(\hat{\Phi}_a^\dagger\hat{\Phi}_b+\hat{\Phi}_b^\dagger\hat{\Phi}_a), \tag{4.7}$$

where γ is assumed real. Since this is proportional to the detector efficiency, it represents the detected quadrature and consequently its noise also scales with the powers of the detector efficiency. The shot noise also decreases with detector efficiency but only linearly. That is, the N-photon counting probability is proportional to η^N so that the two-photon correlations important in squeezing decrease linearly with η when they are scaled to the shot noise level. From now on take $\gamma=1$ since it is now clear what the physical effect of reduced detector efficiency has on making quantum limited measurements such as in pulsed squeezing experiments.

The two-photon coincidence rate is

$$G^{(2)}(t,t')=\langle:\hat{I}_0(t)\hat{I}_0(t'):\rangle+\langle:\hat{X}(t)\hat{X}(t'):\rangle+\langle:\hat{I}_0(t)\hat{X}(t')+\hat{X}(t)\hat{I}_0(t'):\rangle \tag{4.8}$$

and $\hat{I}_0=(\eta_a r^2-\eta_b t^2)\hat{I}_a+(\eta_a t^2-\eta_b r^2)\hat{I}_b$. It is worth noting that for a perfectly balanced system only the last term in Eq. (32) is nonzero. In order to take into account the frequency response of the detectors one can define a detector response function

$$J(\omega)=\frac{1}{\sqrt{2\pi}}\int e^{i\omega t}J(t)dt, \tag{4.9}$$

where $J(t)$ is the current pulse for a photon detection event. Typically, $J(t)$ is taken to be $Ze\,\delta(t)$ where Z is the number of electrons per current pulse. Hence the photocurrent power spectrum is given by

$$P(\omega)=\frac{2\pi}{T}|J(\omega)|^2\overline{G}(-\omega,\omega)=|J(\omega)|^2\left[\overline{I_-^c}+\frac{2\pi}{T}[\langle:\hat{I}_0(-\omega)\hat{I}_0(\omega):\rangle+\langle:\hat{I}_0(-\omega)\hat{X}(\omega)+\hat{X}(-\omega)\hat{I}_0(\omega):\rangle]+\frac{2\pi}{T}\langle:\hat{X}(-\omega)\hat{X}(\omega):\rangle\right]. \tag{4.10}$$

For convenience one can define a power spectrum normalized to the dc detector spectral response giving

$$\mathcal{P}(\omega)=\mathcal{J}(\omega)\left[\overline{I_-^c}+\frac{2\pi}{T}[\langle:\hat{I}_0(-\omega)\hat{I}_0(\omega):\rangle+\langle:\hat{I}_0(-\omega)\hat{X}(\omega)+\hat{X}(-\omega)\hat{I}_0(\omega):\rangle]+\frac{2\pi}{T}\langle:\hat{X}(-\omega)\hat{X}(\omega):\rangle\right], \tag{4.11}$$

where $\mathcal{J}(\omega)=|J(\omega)|^2/|J(\omega=0)|^2$.

In principle, the noise spectrum can be reduced to

$$\mathcal{P}(\omega)=\mathcal{J}(\omega)\left[\overline{I_-^c}+\frac{2\pi}{T}\langle:\hat{X}(-\omega)\hat{X}(\omega):\rangle\right]. \tag{4.12}$$

The last term represents the additional noise above the shot noise level. One should not lose track of the fact that here the last term represents phase-dependent noise correlations and is referred to herein as the squeezing spectrum given by

$$\frac{2\pi}{T}\langle:\hat{X}(-\omega)\hat{X}(\omega):\rangle. \tag{4.13}$$

One can calculate this directly using the positive-P representation as ensemble averages correspond to normally ordered moments.

It is convenient to calculate a normalized squeezing spectrum such that the minimum value of the correlation function is -1. The lower bound is determined from the commutator of the $\hat{X}(t)$ operators, in particular,

$$:\hat{X}(t)\hat{X}(t'):=\mathcal{T}\{\hat{X}(t)\hat{X}(t')+\hat{\Phi}_a^\dagger(t)[\hat{\Phi}_b^\dagger(t'),\hat{\Phi}_b(t)]\hat{\Phi}_a(t')+\hat{\Phi}_b^\dagger(t)[\hat{\Phi}_a^\dagger(t'),\hat{\Phi}_a(t)]\hat{\Phi}_b(t')\}, \tag{4.14}$$

where $\mathcal{T}$ denotes time ordering. Also, since $\hat{X}(t)$ does not contain products of the form $\hat{\Phi}_i^\dagger\hat{\Phi}_i$ the product $\hat{X}(t)\hat{X}(t')$ generates a symmetrically ordered combination appropriate for calculations using the Wigner representation. Since $\langle\hat{X}(-\omega)\hat{X}(\omega)\rangle\geqslant 0$ one has in the positive-P representation

$$\langle X(-\omega)X(\omega)\rangle\geqslant-\frac{1}{2\pi}\left\langle\int_{-T/2}^{T/2}dt(\Phi_a^\dagger\Phi_a+\Phi_b^\dagger\Phi_b)\right\rangle. \tag{4.15}$$

Now one can define the pulsed squeezing spectrum as

$$S(\omega)=\frac{2\pi\langle:\hat{X}(-\omega)\hat{X}(\omega):\rangle}{\langle\int_{-T/2}^{T/2}dt(\hat{\Phi}_a^\dagger\hat{\Phi}_a+\hat{\Phi}_b^\dagger\hat{\Phi}_b)\rangle}. \tag{4.16}$$

Then in the positive-P representation we have

$$S^P(\Phi_S,\xi,\omega)=\langle\hat{S}^P(\Phi_S,\xi,\omega)\rangle=\frac{2\pi\langle X(\xi,-\omega)X(\xi,\omega)\rangle}{\langle\int dt[\Phi_{\rm LO}^\dagger\Phi_{\rm LO}+\Phi_S^\dagger\Phi_S]\rangle}, \tag{4.17}$$

where Φ_S is the signal field and $\Phi_{\rm LO}$ is the local-oscillator field.

In the Wigner representation, the stochastic moments correspond to symmetrical operator ordering resulting in the stochastic moment $\langle X(-\omega)X(\omega)\rangle$ being non-negative. The squeezing spectrum in the Wigner representation is then

$$S^W(\Phi_S,\xi,\omega)=-1+\frac{2\pi\langle X(\xi,-\omega)X(\xi,\omega)\rangle}{\langle\int dt[|\Phi_{\rm LO}|^2+|\Phi_S|^2-1/(\Delta t)]\rangle}, \tag{4.18}$$

where Δt^{-1} is the frequency cutoff. In the case of the hybrid method applied to parametric down-conversion the hybrid spectrum is constructed from

$$S^{\rm hybrid}(\xi,\omega)=\langle\hat{S}^P(\Phi_1,\xi,\omega)-\hat{S}^P(\Phi_2,\xi,\omega)\rangle+S^W(\Phi_w,\xi,\omega). \tag{4.19}$$

In order to specify how the beam splitter input fields relate to actual source fields, the type of experiment has to be more clearly defined. Two different detection schemes are used here. One uses an external local oscillator which is typically some fraction of the output from a source laser which is also used, either directly or indirectly, to pump a nonlinear crystal or waveguide to generate the squeezing. This simple method has been employed a number of times in traveling-wave parametric amplifier squeezing experiments. The other approach is to use a Sagnac interferometer as in the soliton squeezing experiments of Rosenbluh and Shelby [30].

A. External local oscillator

Consider a local-oscillator field which can have its global phase altered continuously and independently so that

$$\hat{\Phi}_a=\hat{\Phi}_s,$$

$$\hat{\Phi}_b=e^{i\theta}\hat{\Phi}_{\rm LO}, \tag{4.20}$$

where $\hat{\Phi}_s$ represents the signal field. The term of interest is the Fourier transformed two-time correlation function

$$\begin{aligned}
&\frac{1}{2\pi}\int\int dt\,dt'e^{i\omega(t'-t)}\langle:\hat{X}(t)\hat{X}(t'):\rangle\\
&=\frac{1}{2\pi}\int\int dt\,dt'e^{i\omega(t-t')}\\
&\quad\times\{\langle:\hat{\Phi}_s^\dagger(t)\hat{\Phi}_{\rm LO}(t)\hat{\Phi}_{\rm LO}^\dagger(t')\hat{\Phi}_s(t'):\rangle\\
&\quad+\langle:\hat{\Phi}_{\rm LO}^\dagger(t)\hat{\Phi}_s(t)\hat{\Phi}_s^\dagger(t')\hat{\Phi}_{\rm LO}(t'):\rangle\},\\
&\quad+\frac{1}{2\pi}\int\int dt\,dt'e^{i\omega(t'-t)}\\
&\quad\times\{\langle:\hat{\Phi}_s^\dagger(t)\hat{\Phi}_{\rm LO}(t)\hat{\Phi}_s^\dagger(t')\hat{\Phi}_{\rm LO}(t'):\rangle e^{-i2\theta}\\
&\quad+e^{i2\theta}\langle:\hat{\Phi}_{\rm LO}^\dagger(t)\hat{\Phi}_s(t)\hat{\Phi}_{\rm LO}^\dagger(t')\hat{\Phi}_s(t'):\rangle\}\\
&=\frac{1}{2\pi}\int\int dt\,dt'e^{i\omega(t'-t)}\{\langle:\hat{i}(t)\hat{i}^\dagger(t'):\rangle+\langle:\hat{i}^\dagger(t)\hat{i}(t'):\rangle\\
&\quad+\langle:\hat{i}(t)\hat{i}(t'):\rangle e^{-i2\theta}+e^{i2\theta}\langle:\hat{i}^\dagger(t)\hat{i}^\dagger(t'):\rangle\}.
\end{aligned} \tag{4.21}$$

In the positive-P representation this becomes

$$\langle i(-\omega)i^\dagger(\omega)\rangle+\langle i^\dagger(-\omega)i(\omega)\rangle+\langle i(-\omega)i(\omega)\rangle e^{-i2\theta}+e^{i2\theta}\langle i^\dagger(-\omega)i^\dagger(\omega)\rangle,$$

where $\hat{i}(t)=\hat{\Phi}_s^\dagger(t)\hat{\Phi}_{\rm LO}(t)$. We choose the local-oscillator phase independently for each frequency to maximize the detected squeezing so that

$$\langle i(-\omega)i(\omega)\rangle e^{-i2\theta}+e^{i2\theta}\langle i^\dagger(-\omega)i^\dagger(\omega)\rangle\to-2|\langle i(-\omega)i(\omega)\rangle|. \tag{4.22}$$

The pulsed squeezing spectrum can be calculated using

$$S(\omega)=\frac{4\pi[{\rm Re}\langle i(-\omega)i^\dagger(\omega)\rangle-|\langle i(-\omega)i(\omega)\rangle|]}{\langle\int_{-T/2}^{T/2}dt(\Phi_s^\dagger\Phi_s+\Phi_{\rm LO}^\dagger\Phi_{\rm LO})\rangle}, \tag{4.23}$$

where ${\rm Re}\langle\cdots\rangle$ is the real part of the expectation value.

B. Self-generated local oscillator

In this arrangement a pump and signal pulse are sent into a Sagnac interferometer. The output of the Sagnac interferometer, which contains the nonlinear medium, then consists of a squeezed field and a bright pulse to be used for the local oscillator. These two fields are the input to a homodyne detector as before. Either the signal field or harmonic field can be detected in this way. The difference current is given by

$$\begin{aligned}
\hat{I}_-&=r_{\rm LO}\cos\theta(\hat{\Phi}_1^\dagger\hat{\Phi}_1-\hat{\Phi}_2^\dagger\hat{\Phi}_2)-r_{\rm LO}\sin\theta(\hat{\Phi}_1\hat{\Phi}_2^\dagger+\hat{\Phi}_2\hat{\Phi}_1^\dagger)\\
&=r_{\rm LO}\hat{i}_1\cos\theta-r_{\rm LO}\hat{i}_2\sin\theta,
\end{aligned} \tag{4.24}$$

where $\hat{\Phi}_1$ represents the field transmitted through the beam splitter to form the squeezed vacuum and $\hat{\Phi}_2$ represents the

field transmitted through the beam splitter to form the local oscillator and r_{LO} is the reflectance of the mirror which redirects the field reflected by the Sagnac interferometer into the homodyne detector. In the positive-P representation the difference current correlation is

$$\frac{1}{2\pi r_{\mathrm{LO}}^2}\int\int dt\,dt'\,e^{i\omega(t'-t)}\langle I_-(t)I_-(t')\rangle$$
$$=\cos^2\theta\langle i_1(-\omega)i_1(\omega)\rangle+\sin^2\theta\langle i_2(-\omega)i_2(\omega)\rangle$$
$$-\frac{1}{2}\sin 2\theta[\langle i_1(-\omega)i_2(\omega)\rangle+\langle i_2(-\omega)i_1(\omega)\rangle]$$
$$\equiv\cos^2\theta C_{11}+\sin^2\theta C_{22}-\frac{1}{2}\sin 2\theta(C_{12}+C_{21}). \qquad (4.25)$$

As before one can choose the global phase of the local oscillator to maximize the amount of squeezing which is equivalent to finding the minimum value of Eq. (4.25) for each frequency independently and is given by

$$\langle i_1(-\omega)i_1(\omega)\rangle+\langle i_2(-\omega)i_2(\omega)\rangle-\{[\langle i_1(-\omega)i_1(\omega)\rangle-\langle i_2(-\omega)i_2(\omega)\rangle]^2+[\langle i_1(-\omega)i_2(\omega)\rangle+\langle i_2(-\omega)i_1(\omega)\rangle]^2\}^{1/2}.$$

The lower bound is found in the same way as above from

$$:\frac{\hat I_-(t)\hat I_-(t')}{r_{\mathrm{LO}}^2}:=\mathcal{T}\left\{\frac{\hat I_-(t)\hat I_-(t')}{r_{\mathrm{LO}}^2}+\cos^2\theta\{\Phi_1^\dagger(t)\times[\Phi_1^\dagger(t'),\Phi_1(t)]\Phi_1(t')+\Phi_2^\dagger(t)\times[\Phi_2^\dagger(t'),\Phi_2(t)]\Phi_2(t')\}+\sin^2\theta\{[\Phi_1^\dagger(t'),\Phi_1(t)]\Phi_2^\dagger(t')\Phi_2(t)+\Phi_1^\dagger(t)[\Phi_2^\dagger(t'),\Phi_2(t)]\Phi_1(t')\}\right\} \qquad (4.26)$$

so that the pulsed squeezing spectrum can be calculated from

$$S(\omega)=\frac{2\pi[C_{11}+C_{22}-\sqrt{(C_{11}-C_{22})^2+(C_{12}+C_{21})^2}]}{\langle\int_{-T/2}^{T/2}dt(\Phi_1^\dagger\Phi_1+\Phi_2^\dagger\Phi_2)\rangle}. \qquad (4.27)$$

V. RESULTS AND DISCUSSION

A. Parametric down-conversion and matched local oscillators

In parametric down-conversion it is known that for short pump pulses, that is, the pump pulse duration is of the same order as the inverse phase-matching bandwidth, the group-velocity mismatch and group-velocity dispersion both need to be taken into account in determining the properties of the local oscillator. The local oscillator needs to be optimized with respect to its pulse width, phase structure, and temporal overlap with the squeezed vacuum pulse. This has been demonstrated in previous work by the authors [32] by employing in the comoving frame temporally shifted, dispersed local oscillators whose initial pulse width is intermediate between the pump pulse width and the inverse phase-matching bandwidth. The asymmetry introduced by a group-velocity mismatch causes the measured squeezing to change as the shorter local-oscillator pulse is overlapped with different portions of the squeezed vacuum. The phase structure of the local oscillator can be matched in a practical sense with that of the squeezed vacuum through a chirp induced from group-velocity dispersion. Significant squeezing can still be achieved without the optimization of the local oscillator since the underlying instabilities of the $\chi^{(2)}$ nonlinear process result in an exponential growth in fluctuations in some quadrature. This can be seen from an analysis of the stability of cw fields to fluctuations. However, the details of the instabilities in the pulsed case will be different.

To illustrate the spectral features of the squeezing spectrum of the down-converted signal for pump pulses of the same duration and which experience the same dispersion as the following simulton calculations, we plot in Fig. 1 the squeezing spectrum using the Wigner representation for a coherent pump pulse $\mathrm{sech}^2(\tau/5)$ with $k_2''/2k_1''=0.05$, $\bar{n}=10^9$. In these simulations, we assumed equal group velocity and exact phase matching. The local oscillator is chosen to be equal to the initial pump pulse. This is not optimal, but means that the temporal width of the local-oscillator and squeezed signal are comparable as in the following self-generated local-oscillator arrangement used for the simulton calculations. The distinctive spectral features are the subshot noise fluctuations about the carrier frequency and the excess noise sideband peaks. We then repeated the calculation using the positive-P–Wigner hybrid technique, which gives the dc squeezing more exactly. However, for the large value of $\bar{n}$ used here, it turns out that the corrections are much smaller than the error in the Wigner calculation. Hence, the dc squeezing shown in Fig. 2 is the same as depicted in Fig. 1. The dc squeezing shows the characteristic effect of group-velocity dispersion whereby the measured squeezing decreases after propagating several dispersion lengths. Optimizing the local oscillator as discussed earlier reduces this detrimental effect. However, since the combination of nonlinearity and dispersion can induce instabilities which result in squeezing, the problem with dispersion effects is in measuring the squeezing rather than in producing it.

Fundamental solitons of the nonlinear Schrödinger equation can exhibit large quadrature-phase squeezing as well. There the U(1) symmetry of the field provides an invariance to arbitrary phase rotations. The nonlinearity produces an intensity-dependent phase shift called self-phase modulation. As a result quantum noise produces phase diffusion which leads to quadrature-phase squeezing. The interplay between dispersion and nonlinearity leads to modulational instability and an exponential growth in fluctuations about a cw field. However, the soliton is stable to coherent quantum fluctuations. In the case of soliton propagation, the pulse does not temporally broaden during propagation and its intensity spectrum does not change either so the type of local oscillator required will be different compared to the earlier case of parametric down-conversion. This nonlinear Schrödinger soliton squeezing can be measured using the self-generated local oscillator from a Sagnac interferometer. Again this is not optimal but a practical compromise.

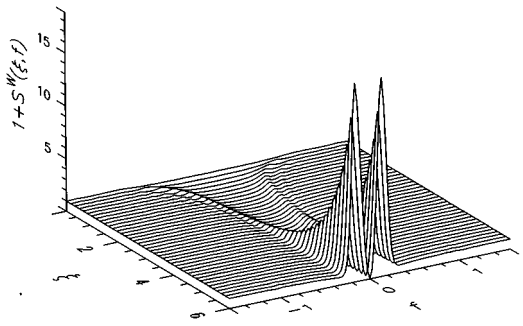

FIG. 1. Squeezing spectrum using the Wigner representation for parametric down-conversion with $k_2''=0.1k_1''$, $z_0(k_0^{(2)}-2k_0^{(1)})=0$.

B. Group-velocity matched simultons

Coherent simultons are coherent states whose temporal profile is given by the solutions to the classical field equations. In particular, we consider the subset of solutions which are the known bright solutions whose analytic form are the coupled temporal sech^2 pulses described elsewhere [3]. These particular solutions satisfy the following simultaneous equations:

$$\phi=\phi_0\mathrm{sech}^2(\kappa\tau)e^{i\theta_1\xi},$$

$$\psi=\psi_0\mathrm{sech}^2(\kappa\tau)e^{i\theta_2\xi},$$

$$\theta_1=-2\kappa^2\mathrm{sgn}(k_1''),$$

$$\theta_2=z_0(k_0^{(2)}-2k_0^{(1)})-2\kappa^2\frac{k_2''}{|k_1''|},$$

$$\theta_2=2\theta_1,$$

$$\psi_0=\frac{-i|k_1''|\phi_0^2}{6\kappa^2k_2''},$$

$$|\phi_0|^2=\frac{18\kappa^4k_2''}{k_1''}.$$

More general solutions exist but this analytic form is convenient for specifying the initial conditions to the quantum calculations to follow.

The hybrid method has been demonstrated above for parametric down-conversion including a quantized, dispersed, depleted pump field [22]. That exact calculation is often approximated in the literature by a pulsed classical pump field which is constant with propagation. However, experiments performed using subpicosecond pulses cannot always be described this way because the nonlinear medium is dispersive and depletion can be important. Also, recent experiments using $LiTaO_3$ waveguides [33] exhibit two-photon absorption of the short pump pulses which provides an additional pump depletion mechanism. Although this has not been considered here it is possible to incorporate these effects in the formulation of the problem used in this paper, if required. Figure 3 shows the corrections due to the quantized, depleted pump for a simulton with $k_2''/2k_1''=0.05$ and $\kappa=0.2$ in the normal dispersion regime. This shows that even when the

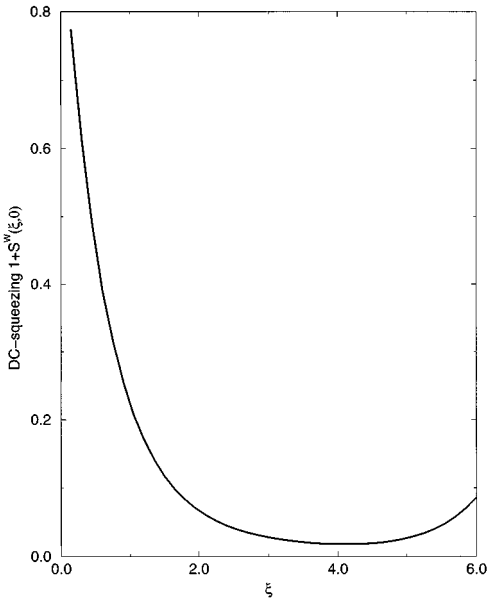

FIG. 2. dc-squeezing using the Wigner method for parametric down-conversion. The parameters correspond to those used in Fig. 1.

group-velocity dispersion at the pump frequency is small compared to the signal group-velocity dispersion and the pump field contains more than 10^9 photons, the pump field quantum dynamics is important. The corresponding dc squeezing calculated using the hybrid method is shown in Fig. 4 of about 5 dB. An important parameter is the ratio of the signal to pump group-velocity dispersion. For these particular solutions, the ratio $k_2''/k_1''=2$ when exact phase matching is used. The phase mismatch required changes sign depending on whether the ratio k_2''/k_1'' is above or below 2. After propagating many dispersion lengths, it is found that the squeezing spectrum measured using the self-generated local-oscillator arrangement is qualitatively different depending on the sign of the phase mismatch. Figures 5 and 6 are Wigner simulations for $k_2''/2k_1''=0.05$ and $k_2''/2k_1''=1.69$. The results suggest that waveguides with a smaller k_2''/k_1'' ratio are better for producing quadrature-phase squeezed simultons for small phase mismatches. By increasing the group-

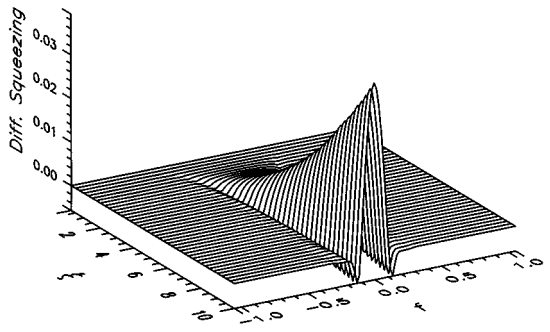

FIG. 3. Quantum corrections for simultons due to the quantized depleted pump versus propagation distance using the positive-P fields ϕ_2,ϕ_1,ψ for $\overline{n}=10^9$. The initial conditions are $\langle\phi_2(0,\tau)\rangle=0.053\,66\mathrm{sech}^2(\tau/5)$, $\langle\psi(0,\tau)\rangle=-0.12\mathrm{sech}^2(\tau/5)$, with $k_2''=0.1k_1''$ and $z_0(k_0^{(2)}-2k_0^{(1)})=-0.152$.

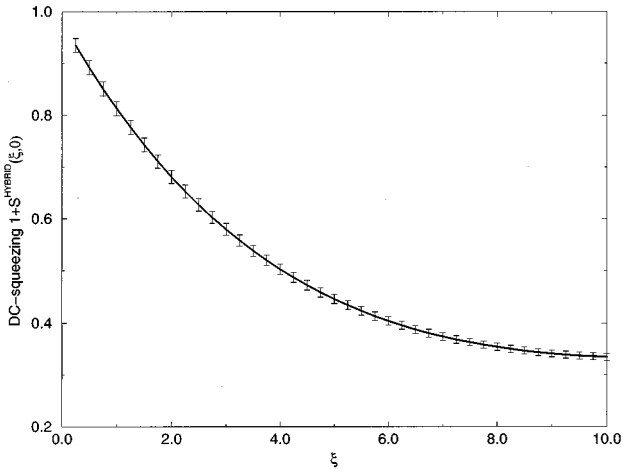

FIG. 4. dc squeezing versus propagation for the simulton initial condition in Fig. 3 using the hybrid positive-P–Wigner method.

velocity dispersion at the fundamental frequency ω_1, the interaction length required is reduced and the k_2''/k_1'' ratio is decreased. However, for the same $k_2''/2k_1''=1.69$ ratio it is possible to use shorter pulses and obtain dc squeezing which persists for longer propagation distances. This is shown in Fig. 7 for the case $\beta=2$ giving $\kappa=1/1.174\,73$ where the phase mismatch $\beta=z_0(k_0^{(2)}-2k_0^{(1)})$. The latter property is not expected for pulses which are not solitary waves.

C. Cascading including phase and group-velocity mismatch

As the ratio k_2''/k_1'' departs from 2, the phase mismatch required increases in magnitude. Therefore we consider the experimentally easier case where the second harmonic is initially in the vacuum state and there is a large phase mismatch between the two carrier frequencies. In this case an approximate cw solution is known analytically for the adiabatically eliminated pump field which follows immediately from the solution to the nonlinear Schrödinger equation. One can see the oscillations in the dc squeezing in Fig. 8 from the phase mismatch and the magnitude of dc squeezing for group-velocity matching is comparable to the earlier case for $k_2''/k_1''=0.1$. Except here the pump dispersion is an average taken from the Sellmeier equations for KTP and RTP at 425 nm [34] so that $\omega_2'^2k_2''/2\omega_1'^2k_1''=1.69$. The effect of group-velocity mismatch can be reduced by increasing the phase-mismatch but for these solutions this requires using higher-intensity pulses. Figure 8 shows the effect of varying the phase mismatch, including the group-velocity mismatch $\Delta v_g=z_0(1/\omega_1'-1/\omega_2')/t_0$, for initial conditions of the form

$$\phi(0,\tau)=\sqrt{2\beta}\,\mathrm{sech}(\tau).$$

This is the fundamental soliton of the nonlinear Schrödinger equation with an effective nonlinearity $1/2\beta$. This configuration appears to be the easiest type of experiment to perform since it relaxes the restrictions on phase matching, group-velocity matching, and correct input fields.

VI. CONCLUSIONS

The squeezing of coherent simultons was demonstrated and the greatest noise reduction was found for the case where

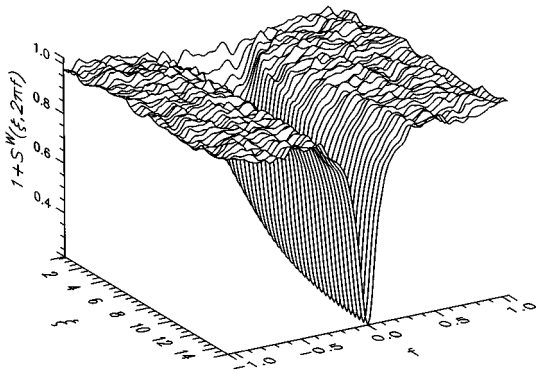

FIG. 5. Squeezing spectrum using the Wigner representation for the simulton initial condition in Fig. 3.

the group-velocity dispersion at the second-harmonic frequency was less than at the fundamental frequency. This appears to be a favorable condition for generation of bright squeezed pulses at the fundamental frequency using simulton propagation for small phase mismatches. The optimal crystal parameters, input conditions, and local oscillator are not known. It is emphasized that no optimization of the local oscillator was carried out for the simulton case as previously investigated for the parametric down-conversion scheme. Note also that materials such as $LiNBO_3$ have a larger positive GVD at the second-harmonic frequency.

It was found that the phase mismatch required for the particular solutions used here was important in determining the low-frequency squeezing for a particular ratio of GVDs. This is obviously true when the group-velocity mismatch is not compensated but was also found for the group-velocity matched case since the solutions we used for initial conditions specify the relationship between pulse duration, dispersion, and phase mismatch. Numerically, solitary solutions are known to exist for more complicated temporal pulses in the case of a group-velocity mismatch [17]. As a first step toward a simulton squeezing experiment, using a large phase mismatch with vacuum input at the second-harmonic frequency is easier experimentally [35], achievable with current KTP waveguides, and allows the variation of the squeezing with phase mismatch to be investigated directly without having to inject the correct amplitude second-harmonic pulse.

The positive-P representation is useful for studying quan-

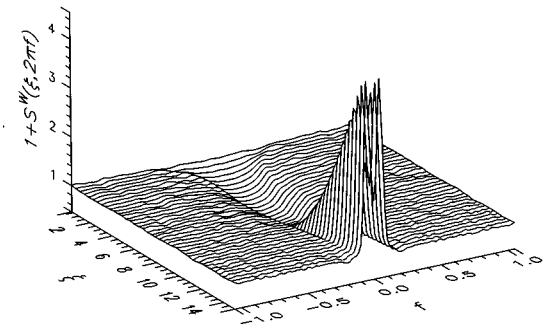

FIG. 6. Squeezing spectrum using the Wigner representation for $k_2''=3.38k_1''$, $z_0(k_0^{(2)}-2k_0^{(1)})=0.1104$, and $\Delta v=0$, $\overline{n}=10^9$. The initial conditions are $\langle\phi_w(0,\tau)\rangle=0.376\,808\,\mathrm{sech}^2(\tau/5)$, $\langle\psi(0,\tau)\rangle=-0.12\,\mathrm{sech}^2(\tau/5)$.

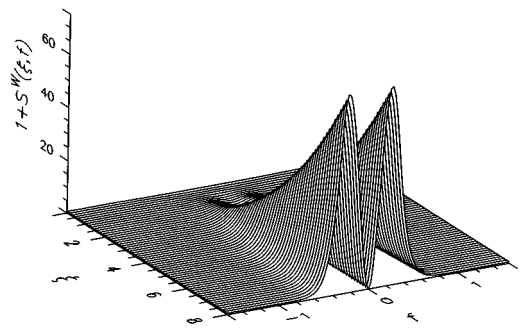

FIG. 7. Squeezing spectrum using the Wigner representation for $k_2''=3.38k_1''$ and $\overline{n}=10^9$. The initial conditions are $\kappa=1/1.174\,73$, $\beta=2$, $\langle\phi_w(0,\tau)\rangle=5.652\,17\,\mathrm{sech}^2(\kappa\tau)$, $\langle\psi(0,\tau)\rangle=-2.173\,91\,\mathrm{sech}^2(\kappa\tau)$.

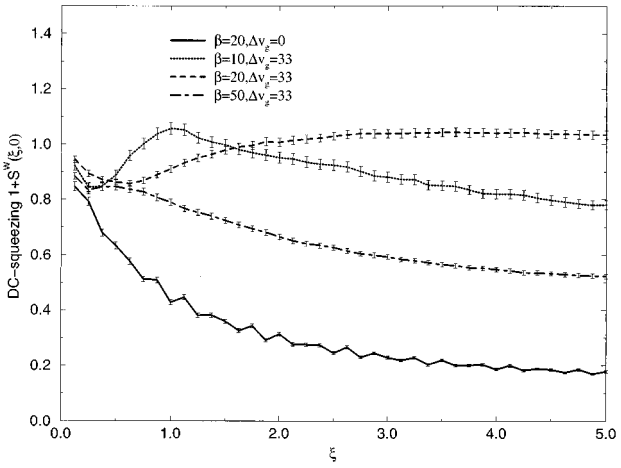

FIG. 8. dc squeezing versus propagation for various phase mismatches with $k_2''=3.38\ k_1''$ using initial conditions $\langle\phi(0,\tau)\rangle^2=2\beta\,\mathrm{sech}^2(\tau)$, $\langle\psi(0,\tau)\rangle=0$, and $\overline{n}=10^9$.

tum field propagation in dispersive nonlinear dielectrics. The quantum statistics of coherent quantum simultons was investigated using a robust algorithm for overcoming difficulties with the use of a nondiagonal coherent state representation. It can be more efficient to solve the exact stochastic equations in combination with an exact Wigner representation of a related problem to calculate the quadrature-phase squeezing spectrum. It is expected that the technique will be useful for studying higher-order quantum correlation functions as well.

[1] R. DeSalvo *et al.*, Opt. Lett. **17**, 28 (1992).
[2] Dmitry E. Pelinovsky, Alexander V. Buryak, and Yuri S. Kivshar, Phys. Rev. Lett. **75**, 591 (1995).
[3] M. J. Werner and P. Drummond, J. Opt. Soc. Am. B **10**, 2390 (1993).
[4] M. J. Werner, Ph.D thesis, University of Queensland, 1994.
[5] D. F. Walls, Nature (London) **306**, 141 (1983).
[6] Y. N. Karamzin and A. P. Sukhorukov, Zh. Éksp. Teor. Fiz. **68**, 834 (1975) [Sov. Phys. JETP **41**, 414 (1976)].
[7] Y. N. Karamzin, A. P. Sukhorukov, and T. S. Filipchuk, Moscow Univ. Phys. Bull. **19**, 91 (1978).
[8] G. Valiulis and K. Staliunas, Lith. Phys. J. **31**, 38 (1991).
[9] M. J. Werner and P. D. Drummond, Quantum Electron. Laser Sci. Tech. Dig. Ser. **12**, 290 (1993).
[10] M. J. Werner and P. D. Drummond, Opt. Lett. **19**, 613 (1994).
[11] H. He, M. J. Werner, and P. D. Drummond, Phys. Rev. E **54**, 896 (1996).
[12] W. E. Torruellas *et al.*, Phys. Rev. Lett. **74**, 5036 (1995).
[13] A. Sizmann (private communication).
[14] L. E. Nelson *et al.*, Opt. Lett. **21**, 1759 (1996).
[15] Yan-Qing Lu *et al.*, Appl. Phys. Lett. **69**, 3155 (1996).
[16] D. K. Serkland, M. M. Fejer, R. L. Byer, and Y. Yamamoto, Opt. Lett. **20**, 1649 (1995).
[17] L. Torner, D. Mazilu, and D. Mihalache, Phys. Rev. Lett. **77**, 2455 (1996).
[18] M. Rosenbluh and R. M. Shelby, Phys. Rev. Lett. **66**, 153 (1991); P. D. Drummond, R. M. Shelby, S. R. Friberg, and Y. Yamamoto, Nature (London) **365**, 307 (1993).
[19] R.-D. Li and P. Kumar, Phys. Rev. A **49**, 2157 (1994).
[20] R.-D. Li and P. Kumar, J. Opt. Soc. Am. B **12**, 2310 (1995).
[21] M. Anderson, M. Beck, M. G. Raymer, and J. Bierlein, Opt. Lett. **20**, 620 (1995).
[22] M. J. Werner and P. D. Drummond, J. Comput. Phys. **132**, 312 (1997).
[23] M. G. Raymer, P. D. Drummond, and S. Carter, Opt. Lett. **16**, 1189 (1991).
[24] P. D. Drummond and S. J. Carter, J. Opt. Soc. Am. B **4**, 1565 (1987).
[25] E. C. G. Sudarshan, Phys. Rev. Lett. **10**, 277 (1963); R. J. Glauber, Phys. Rev. **130**, 2529 (1963).
[26] P. D. Drummond and C. W. Gardiner, J. Phys. A **13**, 2353 (1980).
[27] K. E. Cahill and R. J. Glauber, Phys. Rev. **177**, 1882 (1969).
[28] A. Gilchrist, C. W. Gardiner, and P. D. Drummond, Phys. Rev. A **55**, 3014 (1997).
[29] P. D. Drummond and A. D. Hardman, Europhys. Lett. **21**, 279 (1993).
[30] M. Rosenbluh and R. M. Shelby, Phys. Rev. Lett. **66**, 153 (1991).
[31] P. D. Drummond, *Time Dependent Quantum Correlations and Squeezing*, edited by J. D. Harvey and D. F. Walls, Quantum Optics Vol. V (Springer-Verlag, Heidelberg, 1989).
[32] M. J. Werner, M. G. Raymer, M. Beck, and P. D. Drummond, Phys. Rev. A **52**, 4202 (1995).
[33] M. Anderson and M.G. Raymer (unpublished).
[34] M. G. Roelofs, A. Suna, W. Bindloss, and J. D. Bierlein, J. Appl. Phys. **76**, 4999 (1994).
[35] Ruo-Ding Li and Prem Kumar, Opt. Lett. **18**, 1961 (1993).